

Transforming Thymidine into a Magnetic Resonance Imaging Probe for Monitoring Gene Expression

Amnon Bar-Shir,^{†,‡} Guanshu Liu,^{†,§} Yajie Liang,^{†,‡} Nirbhay N. Yadav,^{†,§} Michael T. McMahon,^{†,§} Piotr Walczak,^{†,‡} Sridhar Nimmagadda,^{||} Martin G. Pomper,^{||} Keri A. Tallman,[⊥] Marc M. Greenberg,[⊥] Peter C.M. van Zijl,^{†,§} Jeff W.M. Bulte,^{†,‡,§,#,∇,○} and Assaf A. Gilad^{*,†,‡,§}

[†]Division of MR Research, ^{||}Russell H. Morgan Department of Radiology, and [‡]Cellular Imaging Section, Institute for Cell Engineering, The Johns Hopkins University School of Medicine, Baltimore, Maryland, United States

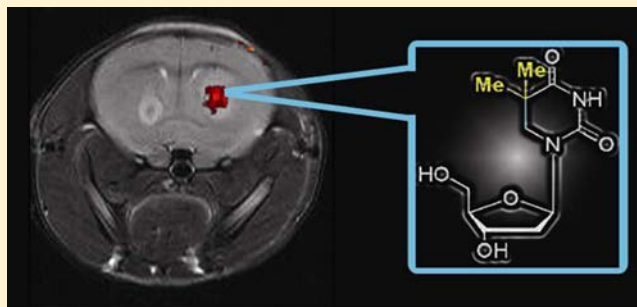
[§]F.M. Kirby Research Center for Functional Brain Imaging, Kennedy Krieger Institute, Baltimore, Maryland, United States

[⊥]Department of Chemistry, [#]Department of Biomedical Engineering, [∇]Department of Chemical and Biomolecular Engineering, and

[○]Department of Oncology, The Johns Hopkins University, Baltimore, Maryland, United States

Supporting Information

ABSTRACT: Synthetic chemistry has revolutionized the understanding of many biological systems. Small compounds that act as agonists and antagonists of proteins, and occasionally as imaging probes, have contributed tremendously to the elucidation of many biological pathways. Nevertheless, the function of thousands of proteins is still elusive, and designing new imaging probes remains a challenge. Through screening and characterization, we identified a thymidine analogue as a probe for imaging the expression of herpes simplex virus type-1 thymidine kinase (HSV1-TK). To detect the probe, we used chemical exchange saturation transfer magnetic resonance imaging (CEST-MRI), in which a dynamic exchange process between an exchangeable proton and the surrounding water protons is used to amplify the desired contrast. Initially, five pyrimidine-based molecules were recognized as putative imaging agents, since their exchangeable imino protons resonate at 5–6 ppm from the water proton frequency and their detection is therefore less affected by endogenous CEST contrast or confounded by direct water saturation. Increasing the pK_a value of the imino proton by reduction of its 5,6-double bond results in a significant reduction of the exchange rate (k_{ex}) between this proton and the water protons. This reduced k_{ex} of the dihydropyrimidine nucleosides fulfills the “slow to intermediate regime” condition for generating high CEST-MRI contrast. Consequently, we identified 5-methyl-5,6-dihydrothymidine as the optimal probe and demonstrated its feasibility for in vivo imaging of HSV1-TK. In light of these findings, this new approach can be generalized for designing specific probes for the in vivo imaging of a variety of proteins and enzymes.



1. INTRODUCTION

Herpes simplex virus type-1 thymidine kinase (HSV1-TK) is a viral enzyme that catalyzes the synthesis of thymidine monophosphate. Compared to mammalian thymidine kinases, HSV1-TK has a lower substrate specificity and thus phosphorylates an array of therapeutics and imaging agents. These applications rely on the entrapment and accumulation of the phosphorylated nucleoside only in cells expressing HSV1-TK.¹ Radiolabeled nucleosides are widely used as imaging probes for HSV1-TK expression with positron emission tomography (PET) and single photon emission computed tomography (SPECT).^{1–4}

The imaging probes for magnetic resonance imaging (MRI) are termed “contrast agents”, since they enhance the water-proton-based contrast between the imaging target and the surrounding tissue. Recently, a new type of contrast mechanism has been developed that exploits chemical exchange saturation

transfer (CEST),^{5–7} to indirectly detect low-concentration solutes through the water signal used for MRI. CEST-MRI contrast is generated by applying a selective radio frequency pulse (saturation pulse) that annihilates the magnetization of specific protons on the solute. Due to dynamic chemical exchange of the “saturated” protons with the water protons and continuous replacement of saturated protons by unsaturated protons followed by renewed saturation, the net magnetization of the water proton is progressively reduced, thus enhancing the MRI contrast. This new contrast mechanism has been used in a range of applications using either diamagnetic (DIACEST) or paramagnetic (PARACEST) agents.^{5,6,8}

CEST contrast is highly dependent on the exchange rate (k_{ex}) of the saturated protons with the water protons. In order

Received: December 18, 2012

Published: January 4, 2013

to achieve the highest contrast and specificity, the k_{ex} should preferably be fast but in the “slow exchange regime” on the NMR time scale, as defined by $k_{\text{ex}} \ll \Delta\omega$, where $\Delta\omega$ is the chemical shift difference between the resonance frequency of the exchangeable protons and the water protons.^{5,6,9} One main drawback of DIACEST agents therefore is the small $\Delta\omega$ between their exchangeable protons (i.e., $\Delta\omega < 4$ ppm for amide, amine, guanidine, and hydroxyl protons) and the water protons. This may lead to deleterious effects from direct saturation of the water protons and increased background signal from endogenous exchangeable protons.^{10–13} The imino proton of pyrimidine-based nucleosides has a $\Delta\omega = 5–6$ ppm,¹⁴ making pyrimidine analogues potentially suitable for CEST imaging. However, the k_{ex} of the imino protons with water is fast ($>3000 \text{ s}^{-1}$) and thus needs to be reduced in order to make these nucleosides ideal CEST-based contrast agents. Changing the acid dissociation constant ($\text{p}K_{\text{a}}$) value of the imino proton of thymidine (dT) by rational chemical modification can be used to modulate its k_{ex} . We therefore modified dT chemically to improve its CEST-MRI properties by increasing the imino proton $\text{p}K_{\text{a}}$ value and reducing its k_{ex} with water to comply with the slow exchange condition on the NMR time scale. The synthetic dT analogue 5-methyl-5,6-dihydrothymidine showed an excellent CEST contrast, as well as high specificity to HSV1-TK, and allowed successful in vivo monitoring of HSV1-TK expression in tumors with MRI.

2. EXPERIMENTAL SECTION

See the Supporting Information text for detailed descriptions of the following methods: (i) simulations of CEST data; (ii) CEST-MRI at 3.0 T clinical MRI scanner; (iii) cell viability assay; (iv) cell uptake assay; and (v) terminal transferase nick-end-labeling (TUNEL) assay.

2.1. CEST Imaging Probes. 5-Methyl-5,6-dihydrothymidine (2) and thymidine glycol (3) were prepared as previously described.^{15,16} Thymidine (dT) and 5-chloro-2'-deoxyuridine (4) were purchased from Sigma–Aldrich, and (5S)-5,6-dihydrothymidine (1) was purchased from Berry & Associates, Inc.

2.2. Cloning. The HSV1-*tk* gene was cloned into pEXP-5-CT (Invitrogen) for expression in *Escherichia coli* (pEXP-5-CT-HSV1-*tk*). For mammalian expression, the gene was cloned into pcDNA3.1 (Invitrogen; pcDNA3.1-HSV1-*tk*) and the pLenti-6-V5/DEST vector (Invitrogen; pLenti-6-HSV1-*tk*), both under a cytomegalovirus (CMV) promoter and a fused V5-tag.

2.3. HSV1-TK Expression and Purification. BL21 (DE3) (Invitrogen) cells were transformed with pEXP-5-CT-HSV1-*tk*. After induction in Magic Media (Invitrogen) at 30 °C for 18 h, the total protein was extracted, and the recombinant HSV1-TK protein fused to the six-histidine tag was purified using cobalt-based immobilized metal affinity chromatography (HisPur cobalt resin, Thermo Scientific). The expression and purity were determined by sodium dodecyl sulfate polyacrylamide gel electrophoresis (SDS-PAGE) and was validated by western blot using an anti-His antibody (Invitrogen).

2.4. Expression in Mammalian Cells. Viruses were propagated in human embryonic kidney 293 cells (HEK-293FT). Forty eight hours after transduction, cells were lysed using Mammalian Protein Extraction Reagent (Thermo Scientific Inc.), and anti-V5 antibody (Invitrogen) was used for immunofluorescence and western blot analyses.

2.5. $\text{p}K_{\text{a}}$ Values. The $\text{p}K_{\text{a}}$ values of the imino protons for the examined molecules were calculated using ChemAxon MarvinSketch v.5.3.3 software (www.chemaxon.com/marvin).

2.6. Kinase Assay. In a solid white 96-well plate, 5 μM substrate (dT, compounds 1, 2, or 3; $N = 4$ for each substrate) and 20 μM ATP were dissolved in 48 μL of kinase reaction buffer (40 mM Tris; pH = 7.5, 20 mM MgCl_2 , and 0.1 mg/mL BSA) followed by the addition of 2 μL of purified HSV1-TK to initiate the kinase reaction. Eight wells without substrate were included as the control reference. The plate

was incubated at room temperature for 2 h, after which 50 μL of Kinase-Glo luciferase reagent (Kinase-Glo max luminescent kinase assay, Promega Inc.) was added. After 30 min, the resulting luminescence values were recorded and used to quantify the residual ATP in the reaction. The relative phosphorylation (%) was then defined as the luminescence signal obtained after the enzymatic reaction (substrate + HSV1-TK + ATP) relative to the signal obtained from wells without substrate (HSV1-TK + ATP). For a phosphorylation assay performed on HEK-293FT lysates, 2 μL of cell extract (either 293^{HSV1-*tk*} or 293^{wt} cells) was used instead of purified HSV1-TK, and the assay was performed using 1 or 2 as the substrate according to the procedure described above.

2.7. In Vitro CEST-MRI. All compounds were dissolved at a concentration of 20 mM in phosphate-buffered saline (PBS) (pH = 7.4) and placed in microcapillaries, as described previously.¹⁷ CEST-MRI experiments were performed on a vertical 11.7 T scanner (Bruker Avance system) at 37 °C. A modified RARE sequence (TR/TE = 10 000/9.4 ms; RARE factor = 16; 1 mm slice thickness; FOV = 11 \times 11 mm²; matrix size = 64 \times 32; resolution = 0.17 \times 0.34 mm²; and NA = 2) including a magnetization transfer (MT) module ($B_1/t_{\text{sat}} = 170 \text{ Hz}/4000 \text{ ms}$) was used to acquire CEST-weighted images from -8 to $+8$ ppm with increments of 0.2 ppm around the water resonance, which was assigned to be at 0 ppm. Pixel-based B_0 correction was used as described before¹⁸ using the same parameters as above except for TR = 1500 ms and $B_1/t_{\text{sat}} = 21 \text{ Hz}/500 \text{ ms}$, with a sweep range from -2 to $+2$ ppm (0.1 ppm steps). Data processing was performed using custom-written scripts in MATLAB (Mathworks). Mean CEST spectra were plotted from an ROI for each sample, after B_0 correction. $\text{MTR}_{\text{asym}} = 100 \times (S^{-\Delta\omega} - S^{+\Delta\omega})/S_0$ was computed at different offsets $\Delta\omega$.

2.8. Quantification of Exchange Rates. Exchange rates were quantified with the saturation power dependent CEST approach (QUESTP) and Bloch equation fitting.¹⁹ For each sample, the MTR_{asym} was measured at the imino resonance frequency for CEST saturation fields of 43, 85, 128, 170, 213, 255, 340, and 426 Hz while the saturation pulse duration was kept constant at 4000 ms. The Bloch equations were then fit numerically to these MTR_{asym} values using MATLAB (Mathworks), and the exchange rates ($k_{\text{ex}}, \text{ s}^{-1}$) were determined from the fits. Errors (95% confidence limits) were estimated using the F statistic.

2.9. Cell Transfection and Transplantation. pcDNA3.1-HSV1-*tk* was used to transfect 9L rat glioma cells. A single clone was selected with 0.5 mg/mL G418 antibiotics. 9L^{HSV1-*tk*} and nontransfected wild type 9L cells (9L^{wt}) were inoculated (2 \times 10⁵ cells/2 μL saline) bilaterally into the striatum of adult NOD-SCID male mice to generate intracranial 9L tumors in both hemispheres.

2.10. In Vivo CEST-MRI. Data were acquired using a horizontal 11.7 T MRI scanner (Bruker, Biospec) equipped with a circular polarized MRI transceiver coil (i.d. = 23 mm). Seven days after cell transplantation, mice were anesthetized with 1.5% isoflurane, and a series of four CEST data sets were obtained at 1, 2, and 3 h following intravenous (iv) injection of 2 in saline (150 mg/kg body). CEST-weighted images were acquired with a modified RARE pulse sequence (TR/TE = 6000/35 ms), using a 213 Hz/4000 ms saturation pulse alternating between ± 5 ppm frequency offsets from the water frequency. For each time point, the MTR_{asym} map was calculated from four pairs of $S^{-5 \text{ ppm}}/S^{+5 \text{ ppm}}$ using MATLAB (Mathworks). A single 1 mm slice with FOV of 1.6 \times 1.6 cm² and a 128 \times 48 matrix was used. To remove magnetization transfer effects, $\Delta\text{MTR}_{\text{asym}}$ was defined as $[\text{MTR}_{\text{asym}}(\text{tumor})] - [\text{MTR}_{\text{asym}}(\text{normal brain tissue})]$ as previously suggested.²⁰

2.11. Immunofluorescent Histology. Mice were transcardially perfused with 10 mM PBS, followed by 4% paraformaldehyde (PFA) fixation. Brains were removed and fixed in 4% PFA overnight, cryopreserved in 30% sucrose, and followed by cryo-sectioning at 30 μm slices. Brain slices were blocked for 1 h at room temperature with PBS containing 5% bovine serum albumin (BSA), followed by overnight incubation in anti-V5 antibody solution. Nuclei were stained using 1 $\mu\text{g}/\text{mL}$ DAPI (Invitrogen).

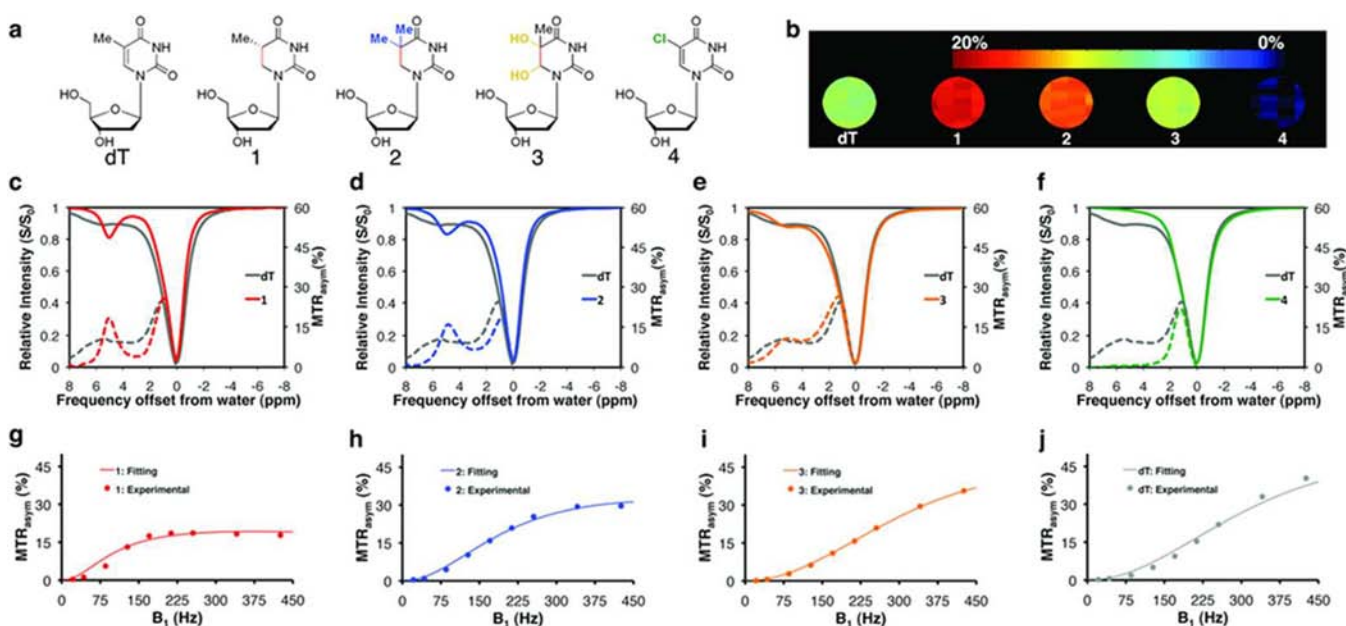


Figure 1. Evaluation of thymidine analogues as potential CEST agents. (a) Chemical structure of dT and compounds 1–4. (b) MTR_{asym} maps of dT and 1–4 obtained at a 5 ppm frequency offset from the water resonance. (c–f) CEST spectra (solid lines) and MTR_{asym} plots (dashed lines). A $B_1 = 170$ Hz was used for b–f. (g–j) MTR_{asym} plotted as a function of saturation power (B_1 , Hz), experimental (dots), and QUESP fitting (lines). In c–j, dT is plotted in gray, 1 in red, 2 in blue, 3 in orange, and 4 in green. Data were acquired at 11.7 T, pH = 7.4, and 37 °C for 20 mM CEST-agent solutions. For 1–3, MTR_{asym} values were calculated at 5 ppm (g–i), and for dT at 6 ppm (j).

2.12. SPECT/CT. An X-SPECT small-animal SPECT/CT system (Gamma Medica-Ideas) was used for image acquisition as previously described.²¹ Briefly, seven days after cell implantation, the mice were injected iv with 50.3 MBq (1.36 mCi) of [¹²⁵I]FIAU. SPECT data were acquired 3 h after radiotracer injection, and the obtained images were coregistered with the corresponding 512 slice CT images. Fused SPECT/CT transaxial sections of 1 mm thickness were generated using Amira 5.2.0 software (Visage Imaging Inc.) showing the SPECT signal obtained from the brain.

3. RESULTS

3.1. Dihydrothymidines Enhance the CEST Contrast In Vitro. Calculated and published pK_a values of the imino proton of dT and four of its analogues (Figure 1a) are summarized in Table 1. Upon hydrogenation of the 5,6-double bond of the pyrimidine ring, the pK_a value of the exchangeable imino proton increases from about 9.8 for dT²² to 11.60 for 5,6-dihydrothymidine (1) due to the loss of the pyrimidine ring

aromaticity. Substitution of the remaining hydrogen at position 5 in 1 with a methyl group produces 5-methyl-5,6-dihydrothymidine (2) and has a negligible effect on the pK_a of its imino proton ($pK_a = 11.57$). The imino proton of thymidine glycol (3) has a pK_a of 11.0, just between dT and compounds 1 and 2, due to its two additional hydroxyl electron-withdrawing groups at the pyrimidine ring. The substitution of the electron-donating methyl group of dT with an electron-withdrawing group, Cl, to generate 5-chloro-2'-deoxyuridine (4), reversed the inductive properties of the 5-substituent and considerably reduced the pK_a value of the imino proton to about 7.9.²³

Using an 11.7 T MRI scanner, we compared the CEST contrast generated by solutions of these four deoxynucleoside analogues in PBS (pH = 7.4, 37 °C) with that of dT. The solid lines in Figure 1c–f represent the CEST spectra, in which the water proton signal (S), normalized by the unsaturated signal (S_0), is plotted as a function of saturation frequency with respect to the water proton resonance frequency. This convention of assigning 0 ppm to the water protons is used in CEST-MRI and should not be confused with proton spectroscopy, in which the water resonance is assigned with respect to tetramethylsilane (TMS) or trimethylsilyl propanoic acid (TSP) and resonates around 4.7–4.8 ppm. The dashed lines represent plots of the asymmetry in the magnetization transfer ratio (MTR_{asym}), a measure of CEST contrast defined by the following: $MTR_{asym} = 100\% \times (S^{-\Delta\omega} - S^{+\Delta\omega})/S_0$, where $S^{-\Delta\omega}$ and $S^{+\Delta\omega}$ are the MRI signal intensities after saturation at $-\Delta\omega$ and $+\Delta\omega$ with respect to the water proton frequency. Taking the signal difference at $-\Delta\omega$ and $+\Delta\omega$ can remove confounding effects due to direct saturation of the water protons. The imino protons of compounds 1–3 showed a local maximum contrast at 5 ppm downfield of the water proton frequency, but only the dihydrothymidines (1 and 2) showed a well-defined sharp peak at that frequency (Figure 1c–f).

Table 1. Properties of dT and Its Analogues

	dT	1	2	3	4
pK_a^a	9.96	11.60	11.57	11.0	7.97
pK_a^b	9.8 ²²	11.6 ⁴³	N.D.	10.7 ⁴⁴	7.9 ²³
k_{ex}^c ($\times 10^3$ s ⁻¹)	5.1 ± 0.7	0.8 ± 0.2	1.7 ± 0.3	3.8 ± 0.2	N.D. ^e
MTR_{asym} (85 Hz)	2%	6%	4%	3%	N.D. ^e
MTR_{asym} (128 Hz)	5%	14%	10%	7%	N.D. ^e
MTR_{asym} (170 Hz)	10%	18%	16%	11%	N.D. ^e
MTR_{asym} (213 Hz)	15%	19%	21%	16%	N.D. ^e

^a pK_a values of the imino proton as calculated using MarvinSketch. ^b pK_a values of the imino proton obtained from the literature. ^cQuantified exchange rates ($\times 10^3$ s⁻¹) of imino and water protons.⁵ ^d MTR_{asym} values (%) at 5 ppm for 20 mM agent. ^eN.D. = not determined.

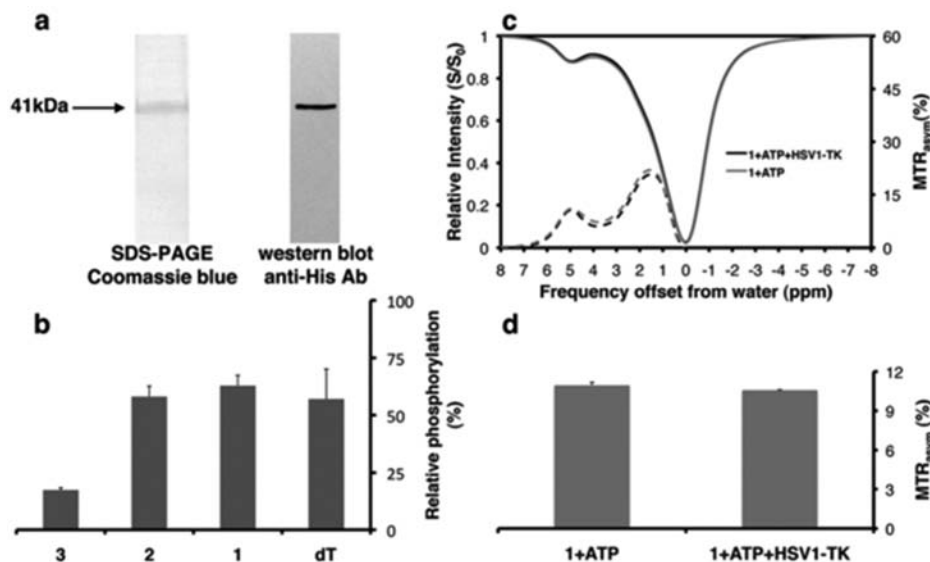


Figure 2. Expression, purification, and activity of HSV1-TK. (a) Coomassie blue staining of SDS-PAGE and western blot analysis (anti-His antibody) of purified recombinant HSV1-TK. (b) Relative phosphorylation of 5 μ M indicated agent (dT, 1–3) in the presence of pure recombinant HSV1-TK (a), as measured with the Kinase-Glo assay. (c) CEST spectra (solid lines) and MTR_{asym} plots (dashed lines) obtained for the kinase reactions with (black lines) and without (gray lines) purified HSV1-TK enzyme for 1. (d) MTR_{asym} (5 ppm) values of 1 before (1 + ATP) and after (1 + ATP + HSV1-TK) phosphorylation ($n = 3$). Relative phosphorylation is defined in the Experimental Section.

Higher exchange rates increase the magnitude of the CEST contrast, which consequently improves the probe's sensitivity. However, if the exchange rate is too fast, the exchanging protons already exchange before being saturated by the CEST labeling pulse. Additionally, for fast exchange rates, the imino and water proton peaks can merge, and thus, the imino signal cannot be distinguished from the water signal. The maximal contrast (slow exchange regime) should be achievable by using an optimal saturation field (B_1) that can be predicted by the expression $B_1(\text{optimal}) = k_{\text{ex}}/2\pi$.²⁴ To assess this, we quantified the k_{ex} in the newly designed probes from the saturation power dependencies of the MTR_{asym} values¹⁹ at 5 ppm for 1–3 and at 6 ppm for dT (Figure 1g–j, Table 1). The imino protons of the two dihydrothymidines, which have the highest pK_a values (1 and 2; Table 1), best fulfill the “slow exchange regime” rule with k_{ex} values of $0.8 \pm 0.2 \times 10^3$ and $1.7 \pm 0.3 \times 10^3$ s⁻¹, respectively, for a chemical shift of $\Delta\omega = 5$ ppm ($=1.6 \times 10^4$ rad/s at 11.7 T). The calculated optimal saturation fields (B_1) were 127 Hz for 1 and 270 Hz for 2. In fact, the MTR_{asym} values of both compounds 1 and 2 reach a plateau at higher B_1 (Figure 1g,h), when saturation fields increase above the optimal value. The imino proton of compound 3 is approaching the intermediate exchange rate range ($k_{\text{ex}} = 3.7 \pm 0.2 \times 10^3$ s⁻¹) and therefore, shows a broadening of the MTR_{asym} curve compared to 1 or 2 (Figure 1c–e). However, as predicted,²⁴ it produces a higher MTR_{asym} if a higher B_1 is used (Figure 1i). No CEST contrast was observed from the imino proton of compound 4 (Table 1, Figure 1b,f), which has the lowest pK_a value (7.97) and falls in the fast exchange regime ($k_{\text{ex}} \gg \Delta\omega$) on the NMR time scale.

The results in Figure 1 were obtained using an MRI scanner operating at field strength of 11.7 T. To evaluate the feasibility of imaging dihydrothymidines at lower field strengths typically used in clinical MRI, we simulated (for dT and compounds 1–3) and performed (dT and 1) CEST experiments at 3 T. The results were compared to simulations and experimental data at 11.7 T. Compounds 1 and 2 fulfill the $k_{\text{ex}} \leq \Delta\omega$ condition at

both 11.7 and 3.0 T and showed a distinct peak at the 5 ppm offset from the water frequency for the two magnetic field strengths (Supporting Information, Figure S1a,b and c,d). In contrast, for 3 and dT, which have a faster exchanging imino proton ($5.1 \pm 0.7 \times 10^3$ and $3.7 \pm 0.2 \times 10^3$ s⁻¹, respectively, Table 1), no peak could be distinguished at the simulated CEST data for the lower magnetic field (Supporting Information, Figure S1d and f), where the $k_{\text{ex}} \leq \Delta\omega$ condition is not fulfilled for $B_0 = 3.0$ T. As mentioned, 1 fulfills the $k_{\text{ex}} \leq \Delta\omega$ condition at 3.0 T and thus produces a visible peak at the 5 ppm offset from the water frequency at the CEST experimental data (Supporting Information, Figure S2b), as has been predicted by the simulations (Supporting Information, Figure S1b). In contrast, for dT, which has a faster exchanging imino proton, no peak could be distinguished and the MTR_{asym} value at 5 ppm obtained for 1 was 40% higher compared to dT (Supporting Information, Figure S2a).

3.2. Dihydrothymidines Are Phosphorylated by HSV1-TK. A major obstacle in designing new imaging probes is to maintain functionality after chemical modification. Therefore, we examined the phosphorylation level of each compound by recombinantly purified HSV1-TK. The HSV1-*tk* gene was subcloned into the pEXP5-CT expression vector in a reading frame with a C-terminal six-histidine tag and subsequently transformed into BL21 (DE3) chemically competent *E. coli*. The recombinant HSV1-TK enzyme was expressed and purified using cobalt-based immobilized metal affinity chromatography (Figure 2a). Notably, the observed phosphorylation of dT and analogues 1 and 2 by purified HSV1-TK was similar (>57%, Figure 2b) after 2 h of incubation in the presence of ATP as the donor phosphate group. However, a lower degree of phosphorylation was observed for 3 (17%, Figure 2b), which may be explained by the hydrophobic nature of the HSV1-TK nucleoside binding site.²⁹ Overall, these results demonstrate that 1 and 2, which yield CEST contrast that is superior to dT, can serve as CEST-based

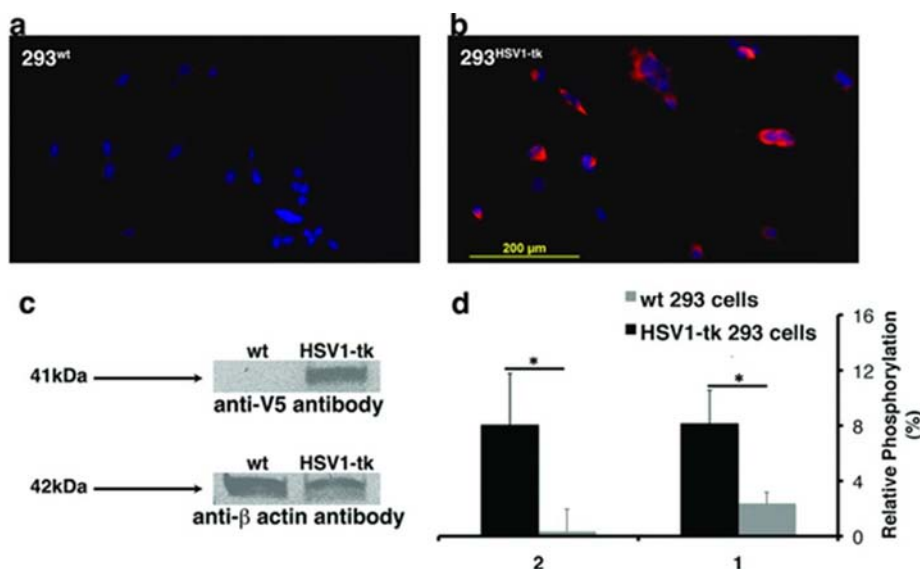


Figure 3. HSV1-TK specificity. Immunofluorescence of (a) 293^{wt} and (b) 293^{HSV1-tk} cells using anti-V5 antibody (red) for HSV1-TK staining overlaid on DAPI staining (blue). (c) Western blot of HEK-293FT cell extracts using anti-V5 antibody, with staining for HSV1-TK-expressing (HSV1-tk) and wild type (wt) cells. (d) Relative phosphorylation of 5 μM compounds 1 and 2 in the presence of 2 μL of cell extracts. Relative phosphorylation is defined in the Experimental Section. **p* < 0.05 (student's *t* test, unpaired, two-tailed).

contrast agents for HSV1-TK, despite their chemical modification.

Next, we examined whether the contrast is affected by phosphorylation. We measured the CEST contrast, with or without purified HSV1-TK, incubated in the presence of ATP for 2 h of incubation at 37 °C (pH = 7.4), followed by 20 min of heat inactivation of the enzyme at 65 °C to end the kinase reaction. Since the phosphorylation site of the substrates is at the 5'-hydroxyl of the deoxyribose moiety, it is expected that the exchange rate of the imino proton and consequently the MTR_{asym} value at 5 ppm would not be affected by phosphorylation. Indeed, the CEST contrast was not affected by phosphorylation, and the MTR_{asym} values at 5 ppm were identical before and after the enzymatic reaction (Figure 2c,d and Figure S3, Supporting Information).

Additionally, we compared the phosphorylation specificity of HSV1-TK to endogenous mammalian thymidine kinases (m-TK) for compounds 1 and 2. Toward that end, we constructed a lentivirus that encodes HSV1-TK under the CMV promoter and transduced HEK-293FT cells (Figure 3a–c). The protein extracts of transduced 293^{HSV1-tk} cells (containing both HSV1-TK and m-TK) and wild type (293^{wt}) control cells (containing m-TK only) were used to measure enzymatic activity in the presence of either 1 or 2. Figure 3d demonstrates that cell extracts containing HSV1-TK exhibited significantly higher phosphorylation of 1 and 2 than control cells. While compounds 1 and 2 had comparable phosphorylation rates, the increase in phosphorylation of 2 with respect to the control extract (293^{wt}) was greater by a factor of about 10 than that of 1, indicating that the additional methyl on position 5, which distinguishes 2 from 1, improves its specificity for HSV1-TK over m-TK. These results are in agreement with the findings that different dT analogues showed variable levels of phosphorylation by m-TK.²⁵ Moreover, it is important to note that such phosphorylation of 2 did not show any toxic effect on the 293^{HSV1-tk} (Supporting Information, Figure S4). This finding is in agreement with previous study showing that dihydrothymidines have no effect on DNA synthesis and do not

increase the rate of mutations.²⁶ In contrast, the antiviral prodrug ganciclovir (GCV) resulted in a cytotoxic effect to the 293^{HSV1-tk} upon phosphorylation (Supporting Information, Figure S4) as predicted and previously reported.²⁷

3.3. Imaging HSV1-TK Activity In Vivo with 2. Next, we evaluated the feasibility of using 2 as a CEST imaging probe for monitoring HSV1-TK in vivo. The rat glioma cell line (9L) was transfected with the expression vector, pcDNA3.1, which encodes HSV1-tk under the regulation of the CMV promoter. Following antibiotic selection, a single clone that showed stable expression levels of the enzyme was selected (9L^{HSV1-tk}). Wild type, nontransfected 9L cells were used as controls (9L^{wt}). The HSV1-TK expression in 9L^{HSV1-tk} cells was confirmed by immunofluorescence (Supporting Information, Figure S5a,b). The HSV1-TK activity was evaluated by an in vitro cell-uptake assay, in which a significant accumulation of the radioactive nucleoside [¹²⁵I]FIAU was observed in 9L^{HSV1-tk} cells after 1 and 3 h of incubation compared to 9L^{wt} cells (Supporting Information, Figure S5c).

Inoculation of 9L^{HSV1-tk} to the ipsilateral striatum and 9L^{wt} into the contralateral striatum of adult male NOD-SCID mice (*n* = 8) resulted in one tumor in each hemisphere of the brain. One week after tumor inoculation, analogue 2 was iv injected, and mice were scanned on a dedicated animal MRI scanner (11.7 T, horizontal bore). Maps of MTR_{asym} were acquired at 1, 2, and 3 h postinjection. Figure 4a shows representative longitudinal MTR_{asym} (5 ppm) maps. As depicted in Figure 4b, 3 h after injection of the probe, the normalized mean MTR_{asym} values (ΔMTR_{asym}) from the 9L^{HSV1-tk} were significantly higher than those obtained from control tumors (4.5 ± 1.5 for 9L^{HSV1-tk} and 2.0 ± 1.7 for 9L^{wt}; *n* = 8; *p* = 0.007). These findings indicate intracellular accumulation (approximately 0.7 mM, Figure S6–S8, Supporting Information) in the 9L^{HSV1-tk} tumors as opposed to clearance from control tumors. Such accumulation of 2 did not induce apoptosis neither in 9L^{HSV1-tk} nor in 9L^{wt} as revealed by terminal deoxynucleotidyl transferase dUTP nick-end-labeling (TUNEL) staining (Supporting Information, Figure S9). The HSV1-TK functionality was

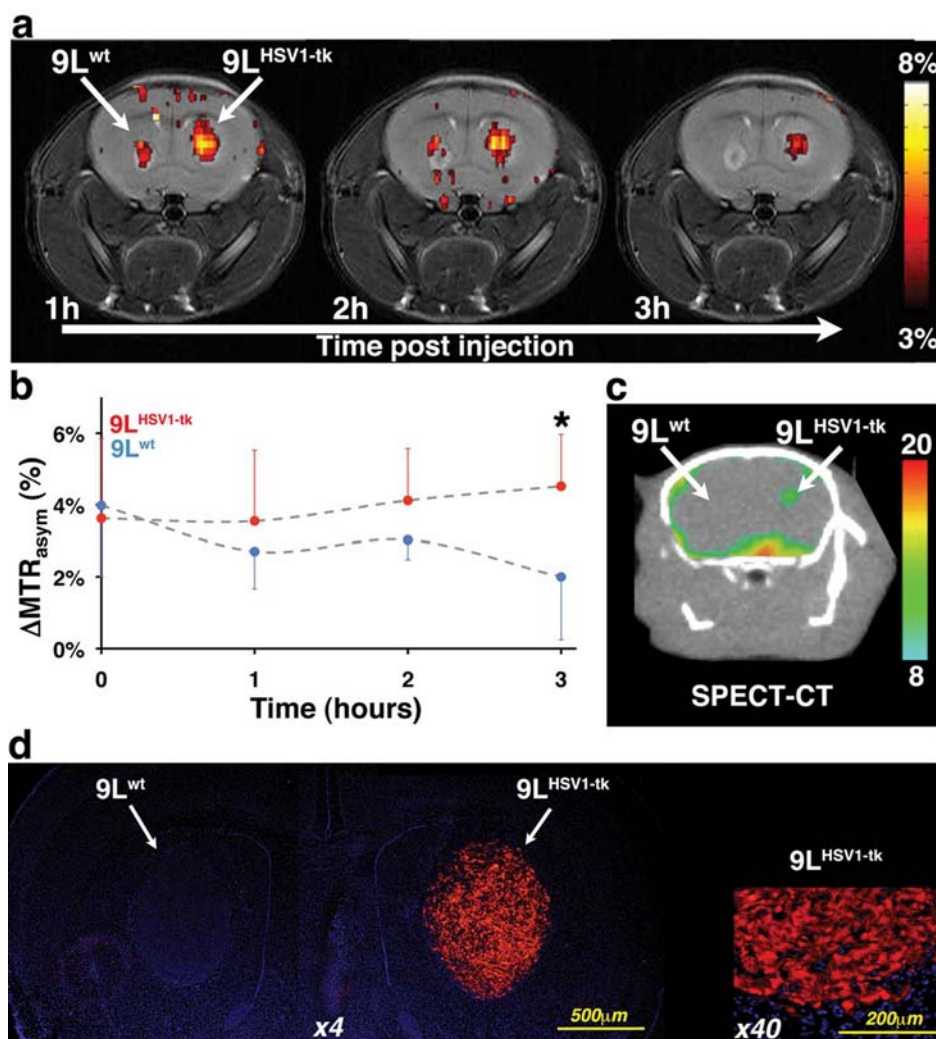


Figure 4. Imaging HSV1-TK expression. Left hemisphere: wild type 9L tumor (9L^{wt}); right hemisphere: 9L tumor expressing HSV1-TK (9L^{HSV1-tk}). (a) Representative longitudinal in vivo MTR_{asyM} (5 ppm) maps of the mouse brain overlaid on T₂-weighted images, showing the distribution of **2** obtained 1, 2, and 3 h after iv injection. (b) Temporal changes in the ΔMTR_{asyM} values (mean ± s.d.) of each tumor type before ($n = 3$) and after ($n = 8$) iv administration of **2**. (* p value < 0.01). (c) Transverse views of coregistered SPECT/CT images of HSV1-TK expression, obtained 3 h after iv injection of [¹²⁵I]FIAU. (d) Immunostaining of perfused mouse brain section. Staining for HSV1-TK (anti-V5 antibody in red) overlaid on DAPI staining (blue) at low (4×) and high (40×) magnifications.

confirmed by the administration of radiolabeled [¹²⁵I]FIAU using SPECT/CT. In agreement with the CEST-MRI results, accumulation of [¹²⁵I]FIAU was observed 3 h after iv injection only at the 9L^{HSV1-tk} tumor (Figure 4c and Figure S10, Supporting Information). The high expression levels of the HSV1-TK in the 9L^{HSV1-tk} tumor was validated by immunofluorescence (Figure 4d).

Overall, these data demonstrate that **2** can be used as an MRI probe to monitor HSV1-TK in vivo.

4. DISCUSSION

We identified **2** as a functional probe for imaging HSV1-TK with CEST. Its exchangeable imino proton, which resonates at Δ ω = 5 ppm, has a considerably lower k_{ex} than parent dT due to its higher pK_{a} value allowing CEST detection with optimal MRI specificity. In addition, while this compound is phosphorylated by HSV1-TK, it is barely phosphorylated by endogenous kinases and therefore allows in vivo MRI of HSV1-tk gene expression with high functional specificity.

Due to the contribution of endogenous proteins and metabolites to in vivo CEST contrast following saturation in the Δ ω range 0–4 ppm from water,^{10–13} it is imperative to design an imaging probe with an exchangeable proton that resonates downfield to this crowded endogenous range. The imino protons of the synthetic deoxynucleosides **1** and **2** not only resonate at Δ ω = 5 ppm but also have a relatively slow k_{ex} compared to that of dT (Table 1) resulting in a well-defined peak centered at the CEST spectra. One advantage over previous generations of CEST reporter genes^{28,29} is that the HSV1-TK CEST-based substrate provides a sharper signal at 5 ppm frequency offset. This makes **1** and **2** favorable DIACEST-based reporters and contrast agents due to less interference from contrast originating in other probes that have exchangeable protons resonating at different frequencies, for example, amide protons at Δ ω ≈ 3.6 ppm,^{13,28} amine protons at Δ ω ≈ 2–2.4 ppm,^{10,29} guanidyl protons at Δ ω ≈ 1.5–1.8 ppm,³⁰ and hydroxyl protons at Δ ω ≈ 0.9 ppm.^{11,12} This may allow simultaneous imaging of multiple targets within the same sample³⁰ and therefore may play an instrumental role in

studying complex biological systems. The reduced k_{ex} values of **1** and **2** allowed CEST detection not only at preclinical MRI scanners operating at high magnetic field (11.7 T in this study) but also at a 3.0 T clinical scanner, where the condition $k_{\text{ex}} < \Delta\omega$ is maintained. However, for clinical MRI scanners, specific absorption rate (SAR) and hardware limitations currently prevent optimal CEST-MRI measurements on low volume samples and small animals. We avoided these limitations in our 3 T experiments by using a pulsed CEST approach;³¹ however, this technique produces less CEST contrast compared to conventional CEST methods. It is important to note that chemical exchange can affect the transverse relaxation as was measured with NMR in solutions containing diamagnetic proteins and metabolites^{32,33} and this property was used for measuring the exchange rate of protein in solution.³³

MRI has been used in the past for studying HSV1-*tk* as a therapeutic gene. The activity of HSV1-TK was measured as the outcome of treatment with GCV as was manifested by changes in T_2 and $T_{1\rho}$.^{34,35} In those cases, the changes were observed within 4 and 2 days respectively. Our results demonstrate that the HSV1-*tk* can be used as an MRI reporter gene for in vivo applications where the reporter activity is measured directly within hours. This is manifested by a statistically significant difference between the CEST contrast produced by 9L^{HSV1-*tk*} and 9L^{wt} tumors, 3 h after injection of compound **2**. It is important to note that the kinetics of the imaging probe may vary between different biological systems or even among individual mice, for instance, due to the heterogeneity of the tumor vasculature, which may alter the accumulation and clearance of the imaging probe. In addition, in order to improve the sensitivity of the suggested system for monitoring enzyme expression, mutated HSV1-TK, which is adjusted to have a higher V_{max}/K_m toward the imaging probe (**2**) and a lower V_{max}/K_m for dT, should be considered, in a manner similar to that applied for the PET imaging of HSV1-*tk* expression.³⁶

Since CEST contrast is visible only when a saturation pulse is applied, it may be used to evaluate multiple genes simultaneously using different MR reporter genes, including CEST reporter genes,^{28,29} paramagnetic MRI reporter genes that alter the transverse relaxation (T_2) of the tissue through accumulation of iron,^{37,38} or MRI-based reporter genes that are designed for either ³¹P- or ¹⁹F-MR spectroscopy.^{39–41} Furthermore, with the recent development of combined PET/MRI high-field scanners,⁴² combining CEST with nuclear imaging could open up new avenues for multimodality molecular and cellular imaging.

5. CONCLUSION

In summary, we have identified an imaging probe that provides frequency-specific MRI contrast with high functional specificity to HSV1-TK. Thus, we have demonstrated, both in vitro and in vivo, the transformation of HSV1-*tk* into an MRI reporter gene. This imaging probe, which is stable for long periods, has the potential to allow serial monitoring of gene expression combined with high-resolution functional and anatomical MRI, as well as in conjunction with nuclear imaging. Overall, the principles outlined in this work may be further extended to a general paradigm for the design and synthesis of new imaging probes for in vivo imaging of a wide range of proteins en route to the elucidation of their biological function.

■ ASSOCIATED CONTENT

📄 Supporting Information

Simulations of CEST data, in vitro imaging using a clinical 3 T MRI scanner, cell viability, in vitro uptake, and apoptosis assays, in vivo CEST-MRI, terminal transferase nick-end-labeling, phosphorylation effect on CEST data, and raw SPECT images. This material is available free of charge via the Internet at <http://pubs.acs.org>.

■ AUTHOR INFORMATION

Corresponding Author

assaf.gilad@jhu.edu

Notes

The authors declare no competing financial interest.

■ ACKNOWLEDGMENTS

Supported by NIH grants EB008769, NS065284, EB005252, EB012590, EB015032, GM-054996, and MSCRF-0103-00. The authors would like to thank Drs. Y. Kato, A.P. Pathak, G. Pelled, J. Xu, C.K. Jones, L. Jiang, K. Glunde, and R.D. Airan.

■ REFERENCES

- (1) Tjuvajev, J. G.; Stockhammer, G.; Desai, R.; Uehara, H.; Watanabe, K.; Gansbacher, B.; Blasberg, R. G. *Cancer Res.* **1995**, *55*, 6126.
- (2) Gambhir, S. S.; Barrio, J. R.; Phelps, M. E.; Iyer, M.; Namavari, M.; Satyamurthy, N.; Wu, L.; Green, L. A.; Bauer, E.; MacLaren, D. C.; Nguyen, K.; Berk, A. J.; Cherry, S. R.; Herschman, H. R. *Proc. Natl. Acad. Sci. U.S.A.* **1999**, *96*, 2333.
- (3) Jacobs, A.; Voges, J.; Reszka, R.; Lercher, M.; Gossmann, A.; Kracht, L.; Kaestle, C.; Wagner, R.; Wienhard, K.; Heiss, W. D. *Lancet* **2001**, *358*, 727.
- (4) Yaghoubi, S. S.; Jensen, M. C.; Satyamurthy, N.; Budhiraja, S.; Paik, D.; Czernin, J.; Gambhir, S. S. *Nat. Clin. Pract. Oncol.* **2009**, *6*, 53.
- (5) Sherry, A. D.; Woods, M. *Annu. Rev. Biomed. Eng.* **2008**, *10*, 391.
- (6) van Zijl, P. C.; Yadav, N. N. *Magn. Reson. Med.* **2011**, *65*, 927.
- (7) Ward, K. M.; Aletras, A. H.; Balaban, R. S. *J. Magn. Reson.* **2000**, *143*, 79.
- (8) Terreno, E.; Castelli, D. D.; Aime, S. *Contrast Media Mol. Imaging* **2010**, *5*, 78.
- (9) Ward, K. M.; Aletras, A. H.; Balaban, R. S. *J. Magn. Reson.* **2000**, *143*, 79.
- (10) Cai, K.; Haris, M.; Singh, A.; Kogan, F.; Greenberg, J. H.; Hariharan, H.; Detre, J. A.; Reddy, R. *Nat. Med.* **2012**, *18*, 302.
- (11) Ling, W.; Regatte, R. R.; Navon, G.; Jerschow, A. *Proc. Natl. Acad. Sci. U.S.A.* **2008**, *105*, 2266.
- (12) van Zijl, P. C.; Jones, C. K.; Ren, J.; Malloy, C. R.; Sherry, A. D. *Proc. Natl. Acad. Sci. U.S.A.* **2007**, *104*, 4359.
- (13) Zhou, J.; Payen, J. F.; Wilson, D. A.; Traystman, R. J.; van Zijl, P. C. *Nat. Med.* **2003**, *9*, 1085.
- (14) Snoussi, K.; Bulte, J. W.; Gueron, M.; van Zijl, P. C. *Magn. Reson. Med.* **2003**, *49*, 998.
- (15) Barvian, M. R.; Greenberg, M. M. *J. Org. Chem.* **1993**, *58*, 6151.
- (16) Greenberg, M. M.; Matray, T. J. *Biochemistry* **1997**, *36*, 14071.
- (17) Liu, G.; Gilad, A. A.; Bulte, J. W.; van Zijl, P. C.; McMahon, M. T. *Contrast Media Mol. Imaging* **2010**, *5*, 162.
- (18) Kim, M.; Gillen, J.; Landman, B. A.; Zhou, J.; van Zijl, P. C. *Magn. Reson. Med.* **2009**, *61*, 1441.
- (19) McMahon, M. T.; Gilad, A. A.; Zhou, J.; Sun, P. Z.; Bulte, J. W.; van Zijl, P. C. *Magn. Reson. Med.* **2006**, *55*, 836.
- (20) Zhou, J.; Lal, B.; Wilson, D. A.; Larterra, J.; van Zijl, P. C. *Magn. Reson. Med.* **2003**, *50*, 1120.
- (21) Nimmagadda, S.; Pullambhatla, M.; Pomper, M. G. *J. Nucl. Med.* **2009**, *50*, 1124.
- (22) Dawson, R. M. C. *Data for Biochemical Research*; Clarendon Press: Oxford, U.K., 1959.

- (23) Theruvathu, J. A.; Kim, C. H.; Darwanto, A.; Neidigh, J. W.; Sowers, L. C. *Biochemistry* **2009**, *48*, 11312.
- (24) Woessner, D. E.; Zhang, S.; Merritt, M. E.; Sherry, A. D. *Magn. Reson. Med.* **2005**, *53*, 790.
- (25) Alauddin, M. M.; Gelovani, J. G. *Curr. Med. Chem.* **2010**, *17*, 1010.
- (26) Evans, J.; Maccabee, M.; Hatahet, Z.; Courcelle, J.; Bockrath, R.; Ide, H.; Wallace, S. *Mutat. Res.* **1993**, *299*, 147.
- (27) Dhar, S.; McConnell, M. P.; Gharibjanian, N. A.; Young, C. M.; Rogers, J. M.; Nguyen, T. D.; Evans, G. R. *Tissue Eng.* **2007**, *13*, 2357.
- (28) Gilad, A. A.; McMahan, M. T.; Walczak, P.; Winnard, P. T., Jr.; Raman, V.; van Laarhoven, H. W.; Skoglund, C. M.; Bulte, J. W.; van Zijl, P. C. *Nat. Biotechnol.* **2007**, *25*, 217.
- (29) Liu, G.; Liang, Y.; Bar-Shir, A.; Chan, K. W.; Galpoththawela, C. S.; Bernard, S. M.; Tse, T.; Yadav, N. N.; Walczak, P.; McMahan, M. T.; Bulte, J. W.; van Zijl, P. C.; Gilad, A. A. *J. Am. Chem. Soc.* **2011**, *133*, 16326.
- (30) McMahan, M. T.; Gilad, A. A.; DeLiso, M. A.; Berman, S. M.; Bulte, J. W.; van Zijl, P. C. *Magn. Reson. Med.* **2008**, *60*, 803.
- (31) Jones, C. K.; Polders, D.; Hua, J.; Zhu, H.; Hoogduin, H. J.; Zhou, J.; Luijten, P.; van Zijl, P. C. *Magn. Reson. Med.* **2012**, *67*, 1579.
- (32) Rabenstein, D. L.; Isab, A. A. *J. Magn. Reson.* **1979**, *36*, 281.
- (33) Zhong, J. H.; Gore, J. C.; Armitage, I. M. *Magn. Reson. Med.* **1989**, *11*, 295.
- (34) Poptani, H.; Puumalainen, A. M.; Grohn, O. H.; Loimas, S.; Kainulainen, R.; Yla-Herttuala, S.; Kauppinen, R. A. *Cancer Gene Ther.* **1998**, *5*, 101.
- (35) Grohn, O. H.; Valonen, P. K.; Lehtimaki, K. K.; Vaisanen, T. H.; Kettunen, M. I.; Yla-Herttuala, S.; Kauppinen, R. A.; Garwood, M. *Cancer Res.* **2003**, *63*, 7571.
- (36) Gambhir, S. S.; Bauer, E.; Black, M. E.; Liang, Q.; Kokoris, M. S.; Barrio, J. R.; Iyer, M.; Namavari, M.; Phelps, M. E.; Herschman, H. R. *Proc. Natl. Acad. Sci. U.S.A.* **2000**, *97*, 2785.
- (37) Cohen, B.; Ziv, K.; Plaks, V.; Israely, T.; Kalchenko, V.; Harmelin, A.; Benjamin, L. E.; Neeman, M. *Nat. Med.* **2007**, *13*, 498.
- (38) Genove, G.; Demarco, U.; Xu, H.; Goins, W. F.; Ahrens, E. T. *Nat. Med.* **2005**, *11*, 450.
- (39) Koretsky, A. P.; Brosnan, M. J.; Chen, L. H.; Chen, J. D.; Van Dyke, T. *Proc. Natl. Acad. Sci. U.S.A.* **1990**, *87*, 3112.
- (40) Walter, G.; Barton, E. R.; Sweeney, H. L. *Proc. Natl. Acad. Sci. U.S.A.* **2000**, *97*, 5151.
- (41) Kodibagkar, V. D.; Yu, J.; Liu, L.; Hetherington, H. P.; Mason, R. P. *Magn. Reson. Imaging* **2006**, *24*, 959.
- (42) Judenhofer, M. S.; Wehrl, H. F.; Newport, D. F.; Catana, C.; Siegel, S. B.; Becker, M.; Thielscher, A.; Kneilling, M.; Lichy, M. P.; Eichner, M.; Klingel, K.; Reischl, G.; Widmaier, S.; Rocken, M.; Nutt, R. E.; Machulla, H. J.; Uludag, K.; Cherry, S. R.; Claussen, C. D.; Pichler, B. J. *Nat. Med.* **2008**, *14*, 459.
- (43) Butler, T. C.; Johnson, D.; Dudley, K. H. *J. Heterocyclic Chem.* **1982**, *19*, 657.
- (44) Iida, S.; Hayatsu, H. *Biochim. Biophys. Acta.* **1971**, *228*, 1.